Available online at www.sciencedirect.com
SCIENCE DIRECT®
Journal of Solid State Chemistry 178 (2005) 1326–1334
JOURNAL OF SOLID STATE CHEMISTRY
www.elsevier.com/locate/jssc

$LaNiO_2$: Synthesis and structural characterization

M. Crespin[a,1], O. Isnard[b,c], F. Dubois[a], J. Choisnet[d], P. Odier[b,*]

[a]Centre de Recherche sur la Matière Divisée, UMR CNRS-Université, 1 B rue de la Férollerie, 45071 Orléans Cedex 2, France
[b]Laboratoire de Cristallographie, CNRS UPR 5031, 25 Avenue des Martyrs, BP166, 38042 Grenoble Cedex 09, France
[c]Institut Universitaire de France, Maison des Universités, 103 boulevard Saint Michel, 75005 Paris, France
[d]CRISMAT, UMR CNRS-ENSICAEN, 6 Boulevard du Maréchal Juin, 14050 Caen Cedex, France

Received 2 September 2004; received in revised form 10 January 2005; accepted 11 January 2005

Abstract

The preparation of a single phase $LaNiO_2$ by controlled H_2 reduction of the perovskite $LaNiO_3$ is reported. The different steps of the synthesis are detailed. The structural characterization is made by X-ray diffraction (XRD) and neutron powder diffraction (NPD) and discussed; the derived crystal structure is the infinite-layer $CaCuO_2$. Both XRD and NPD patterns are characterized by anisotropic shape broadening originating from size effect linked to the reduction process. From NPD, the $LaNiO_2$ powder is composed of platelet-like crystallites having an average thickness equal to 20 nm along the [001] direction. A modulation of the neutron diffraction background is observed and discussed in connection to the reduction process.

Keywords: $LaNiO_2$; Nickel monovalent; Controlled reduction

1. Introduction

The use of topotactic transformations is an interesting and energetically economic way to manipulate chemical species at low temperature. For example, it allows to synthesize $BaTiO_3$ at a few hundred °C [1] or to transform the goethite FeO(OH) oxyhydroxide into Fe_2O_3 hematite by mecano-chemical reaction [2]. It is also efficient to introduce order in solid matter, for example in Li manganate [3] for electrochemical applications or in double perovskite manganites with colossal magneto resistance properties [4]. Oxygen intercalation–de-intercalation also belongs to topotactic-type reactions; it has been widely used to produce new phases or metastable phases with novel electronic and chemical features [5] and mixed-valence [6].

Ni(I) has been discovered in solid state, 20 years ago by Crespin et al. [7] by operating a topotactic reduction of the perovskite $LaNiO_3$, with a controlled H_2 reduction loop at moderate T (~250–450 °C). The authors identified the nickelite $LaNiO_2$ containing formally Ni(I), as deriving from $LaNiO_{2.5}$, the phase issued from the first step of the reduction. Because Ni(I) $3d^9$ is isoelectronic with Cu(II), the key element for high T_c superconductivity, some interest was devoted to synthesize Ni(I) containing oxides with structures similar to those where superconductivity is observed. Hence, several new phases involving Ni(I) in K_2NiF_4 derived structure were obtained: $La_{1.6}Sr_{0.4}NiO_{3.47}$, $LaSrNiO_{3.1}$ [8,9], $La(Ni_{1-x}Al_x)O_{2+x}$ [10]. Manthiran et al. [11] discussed the factors influencing the stabilization of Ni(I) in perovskite-related oxide $A_{n+1}Ni_nO_{3n+1}$. They stressed that "bond length matching between the stretched Ni^+–O and A–O bond to minimize the internal stress and coordination preference and size of the A cations are found to play an important role in accessing Ni^+". As another example, the strongly reduced nickelite $Nd_4Ni_3O_8$ is the triple-[NiO_2] layer, intermediate between the T'-type and the infinite layer type where all the Nd atoms are in a cubic coordination

*Corresponding author. Fax: +33 4 76 88 10 38.
E-mail address: philippe.odier@grenoble.cnsr.fr (P. Odier).
[1]Retired from CNRS.

0022-4596/$ - see front matter © 2005 Elsevier Inc. All rights reserved.
doi:10.1016/j.jssc.2005.01.023

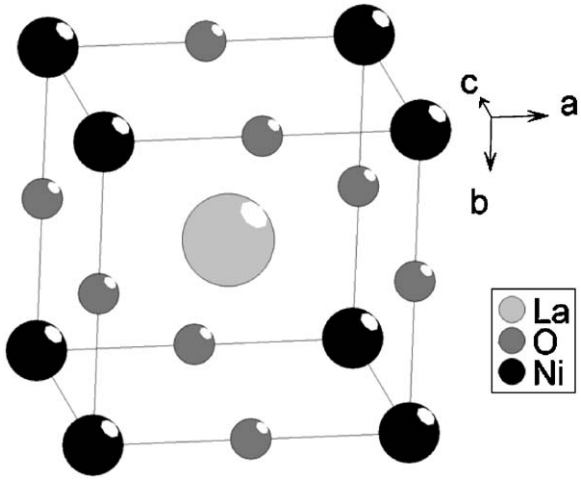

Fig. 1. Structure of $LaNiO_2$ initially proposed by Crespin et al. [7] and isotype to the "∞ layer".

[12,13]. Recently, Ni(I) and Cu(II) where shown to coexist in $LaNi_{0.5}Cu_{0.5}O_{2.25}$ [14].

In the first report [7], $LaNiO_2$ was assumed to have the very simple structure of (Ba,Ca)CuO_2, the so called "∞ layer" discovered later [15], see Fig. 1. Several unsuccessful attempts to reproduce the experiment of Crespin et al. have blown, however, some doubt on the existence of the $LaNiO_2$ phase. Hayward et al. [16] using NaH, the most powerful reducing agent, succeeded some years ago to reduce $LaNiO_3$ at a sufficiently low temperature to avoid the decomposition of $LaNiO_2$. By neutron powder diffraction (NPD), they confirmed the structure predicted initially, but due to a rather imperfect sample, i.e., it had a composition $LaNiO_{2+x}$ and therefore was not fully reduced, they were forced to work a complicated procedure to fit the data. Despite the progress obtained by Hayward et al., the problem of the synthesis of pure $LaNiO_2$ still remains questionable. This motivated us to have a better insight on the first method of synthesis and to obtain a sample as pure as possible.

This paper reports our successful attempt to reproduce the initial experiment of synthesis of $LaNiO_2$, but this time with a sufficiently large amount of powder to allow an NPD study.

2. Experimental

2.1. Reduction vessel

The apparatus was described in Ref. [7] but no details were given at that time on the operational mode, which is described now. To help the reader, we show on Fig. 2 a draw of the vessel. It is composed of a circulated glass loop (1) (volume close to 380 cm^3), a volumetric measurement vessel (2), a reaction cell (3) and a liquid nitrogen trap (4). The reaction cell can be heated and isolated from the circulated loop. The system can be pumped (primary and secondary vacuum, (5)) and filled with He, H_2, O_2, N_2 (6) or other gases.

The volumetric measurement is based on the use of a gas burette system containing five spheres of different known volumes. A reservoir of mercury is used to modify the free volume of the burette; the pressure is measured by a mercury manometer. The determination of a volume of the loop (a fraction of it or its totality) simply uses the Boyle–Mariotte's law and is given by

$$V_x = \frac{P_n b_n}{P_0 - P_n}, \tag{1}$$

where V_x is the unknown volume of glass in standard conditions (stp). P_0 is the pressure of gas when the burette is full of mercury (volume b_0), P_n is the pressure when the nth sphere is filled with gas and b_n is the volume of the nth sphere ($b_0 = b_1 + b_2 + \cdots b_n$). In the actual system $b_1 = 3.650\,cm^3$, $b_2 = 13.890\,cm^3$, $b_3 = 33.900\,cm^3$, $b_4 = 80.730\,cm^3$, and $b_5 = 188.950\,cm^3$, all being measured with a high precision leading to an error in the range of $\pm 1 \times 10^{-3}\,cm^3$.

The gas volume at room temperature is

$$V_{gas} = V_x(P_x 273.16)/(760T), \tag{2}$$

where P_x is the pressure of gas for the volume V_x, and $T(K)$ is the ambient temperature.

The experiment is conducted as follows. Typically, 500 mg of powder is poured in a dense alumina boat that was previously outgassed. After introducing the sample in the reaction cell, it is treated for 12 h at 400 °C under dry oxygen flow to remove all traces of organic residue and fully oxidize the sample, and then the system is out gazed under vacuum at 150 °C max. The volume of the loop is then measured with He as indicated above; it includes the sample cell heated at the temperature of the reducing experiment, the cold trap and the circulating loop. The sample cell is then isolated and a given volume of H_2 introduced in the vessel and measured in stp (the amount of introduced H_2 at starting is 3 to 4 times more than required for the total reduction). H_2 is further introduced in the circulating loop to react with the sample; the water vapor formed being trapped in the cold trap. Pressure is measured versus time; it is a measure of the H_2 consumption and gives access to the progress of the reduction process and to its kinetics. Both volume and pressure can be measured with a very low uncertainty, allowing a good precision even for small volumes. Typically, a volume of 0.1 cm^3 can be measured with a precision of 5%. This ensures a rather accurate follow-up of the de-oxygenation kinetics and of the oxygen stoichiometry, as well. As a result, the error in the oxygen stoichiometry factor is estimated to be ± 0.015 oxygen.

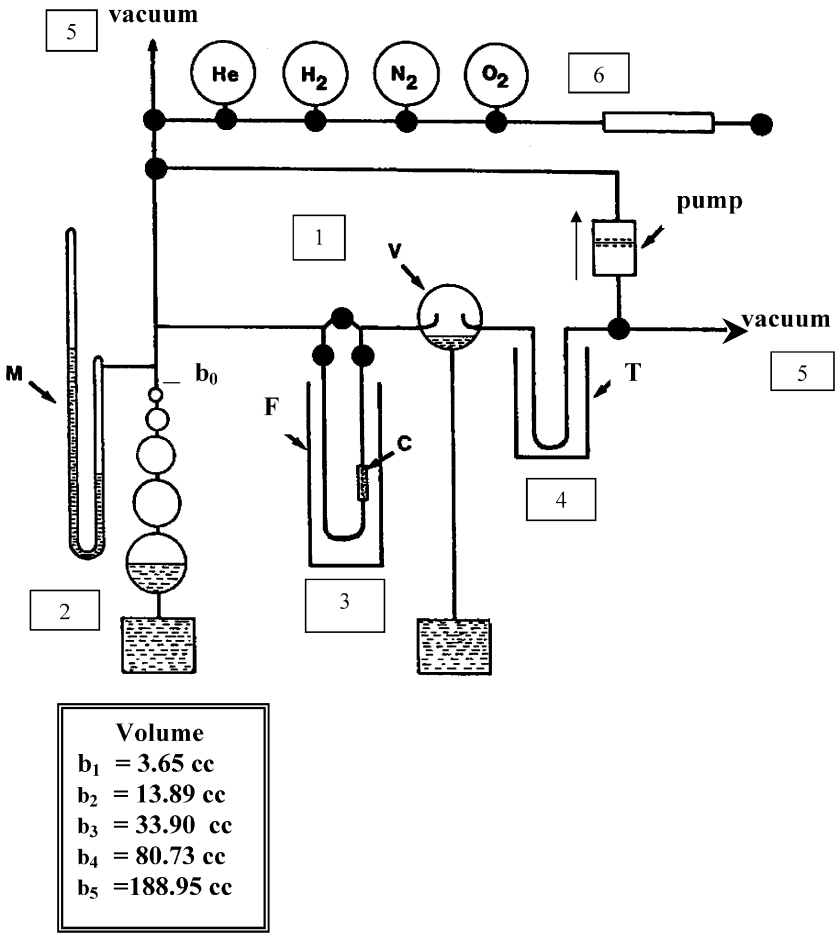

Fig. 2. Reactor for reduction experiments.

2.2. Sample preparation

A batch (10 g) of $LaNiO_3$ powder is prepared by a sol–gel method using acrylamid gelification. This method has been already reported for $LaNi_{0.5}Cu_{0.5}O_3$ phase [17]. It allows to obtain fine particles (<100 nm) with the exact stoichiometry. The $LaNiO_3$ phase is obtained pure at 800 °C under pure oxygen flow with the typical unit cell. To complete its crystallization, it is heated to 950 °C under oxygen flow and slowly furnace cooled, no line broadening can be detected on such sample with our D5000 apparatus (line width ~0.15°).

The initial oxygen stoichiometry of the sample is always measured as a preliminary step by using the previous procedure; it is close to O_3 in the present case (within the experiment error) asserting the quality of both sample and experimental procedure.

2.3. Structural characterization

The neutron diffraction experiments is performed at the Institut Laue Langevin (*I.L.L.*), Grenoble, France, on the *D1B* instruments operated by the *CNRS* whose detailed description can be found elsewhere [18]. A cylindrical vanadium sample holder of 6 mm inner diameter is used. The room temperature diffraction patterns are recorded over an angular range of 80° (2θ), using a multidetector with a step of 0.2° between each of the 400 ^{3}He detection cells. In this configuration, the *D1B* instrument is operating with a wavelength of $\lambda = 1.28$ Å selected by the (311) Bragg reflection of a Ge monochromator, the take off angle being 44.2° 2θ at this wavelength. The data are analysed with the Rietveld structure refinement FULLPROF program [19]. Guidelines of the Rietveld refinement can be found elsewhere [20]. The neutron scattering lengths $b_{Ni} = 1.030 \times 10^{-14}$ m, $b_{La} = 0.824 \times 10^{-14}$ m, $b_O = 0.580 \times 10^{-14}$ m values are taken from Ref. [21].

X-ray powder diffractions have been recorded either in the reflection or transmission mode in a D8 (Brucker) and D5000 (Siemens) apparatus, respectively, the wavelength was that of Cu$K\alpha_1$ (Ni filtered).

3. Results and discussion

Typical results of de-oxygenation versus time are shown onto Fig 3. It shows plots of oxygen

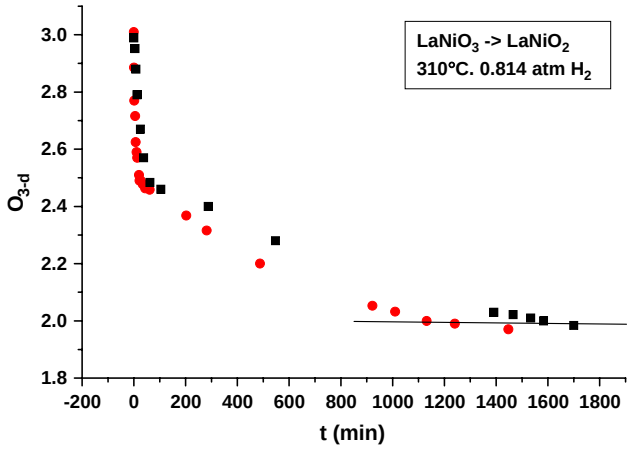

Fig. 3. Kinetics of de-oxygenation of $LaNiO_3$ at 310 °C under an initial H_2 pressure of 0.5 atm.

stoichiometry calculated from the H_2 consumption versus time for two samples operated under identical conditions, i.e., $T = 310$ °C—$P_{H_2} \sim 0.500$ atm H_2—initial weight ~400 mg. The de-oxygenation occurs in two steps of very different kinetics. The first one is very rapid, it lowers the oxygen stoichiometry down to $O_{2.5}$ and give rises to $LaNiO_{2.5}$ [22]. This has been confirmed in a preliminary experiment of a reduction in situ followed by NPD. The second de-oxygenation step is lengthier and tends progressively to the formation of $LaNiO_2$ after 1500 min (25 h) at 310 °C. At this level, the hydrogen pressure reaches ~0.400 atm. Note that in the course of the reduction we could maintain a constant pressure of H_2 by increasing the level of mercury in the reservoir **V** (Fig. 2) and then perform the reduction at constant pressure. However, after each measurement of pressure, the value of b_0 must be measured again and then, the circulation in the loop has to be stopped for some time. This makes more difficult to follow-up the reduction kinetics, especially in its fast regime. According to our experiments, this does not change the kinetics if the reduction of pressure is small, that is the case here.

The structure of the reduced phase is checked by X-ray diffraction. For small samples, typically $\leqslant 500$ mg, a pure $LaNiO_2$ phase is obtained and this result is reproducible. Attempts to produce larger batches of pure $LaNiO_2$ powders (1–3 g) were undertaken but failed. We have tried to find the optimal temperature. When the temperature is too low, i.e., a few degrees below $T = 310$ °C, the kinetics is considerably lowered and even after a week, the reaction is not finished, the product being composed of $LaNiO_{2.5}$ and other phases. On the other hand, if the temperature is raised even a few degrees above 310 °C, the reduction invariably yields to uncontrolled and significant amounts of Ni and La_2O_3 in addition to $LaNiO_2$. The crucial point to access the pure phase is the first step of the reaction, i.e., the formation of $LaNiO_{2.5}$. From several experiments, we have observed that the first step is exothermic and then if a too large batch is reduced, the sample overheats, leading to an uncontrolled product of reaction. Probably, a rate-controlled synthesis should be a useful method for further experiments. In any case, when using a small mass of sample (~500 mg), the right temperature (310 °C), a low heating rate (<50 °C h^{-1}), a low pressure of gas (not higher than 0.6 atm H_2), and a sufficiently large depression (2.5×10^{-3} atm) at the circulating pump, reproducible pure samples of $LaNiO_2$ phase can be produced. To get a sufficient amount of product for NPD, we mixed six samples of smaller amount but of quasi-identical quality. The X-ray diffractogram of Fig. 4 is obtained from such a large batch (3 g). It is clear that all lines index within the $LaNiO_2$ tetragonal cell, as reported initially in Ref. [7]. NPD is performed on that batch of powder and reported Fig. 5. From that diffractogram, it is detected some Ni impurities but not accompanied with La_2O_3.

3.1. Structural analysis

It seems to be clear that this diffraction pattern is featured by rather broad reflections, certainly much broader than that observed for a well-crystallized oxide such as Al_2O_3 (Fig. 6). Even more, the line shape broadening is not constant over the reciprocal space but depends upon the (*h*,*k*,*l*) values. This feature has been also noticed by X-ray diffraction (transmission mode). Fig. 7 shows the full width at half maximum (FWHM) of the different reflections pointing to a differentiation between (*hk*0) and the other (*hkl*) indexes. Note that the error in the experiment bar is in the range of 0.1°.

Such an anisotropic line shape broadening led to difficulties in the Rietveld analysis. A detailed analysis of the systematic broadening as function of (*hkl*) led us to conclude that this is due to a size effect. The (00l) reflections are exhibiting the largest FWHM as can be seen from XRD (Fig. 7) and from NPD (Fig. 5). Modelling the anisotropic broadening involves the hypothesis that the correlation length for coherent crystallites is finite along the *c*-axis and infinite within the (001) plane. The integral width (β_{hkl}, corrected for instrumental resolution) of a Bragg reflection for a small crystallite size is given by the Scherrer formula:

$$\beta_{hkl} = \lambda / D_{hkl} \cos\theta, \tag{3}$$

where λ is the wavelength, θ is the Bragg angle and D_{hkl} is the average diameter (for the all volume of the sample) in the direction normal to the (*hkl*) planes as defined in Ref. [23]. The instrument resolution is obtained from the fit of the Al_2O_3 diffraction pattern given in Fig. 6. If D is the average thickness (over the volume of the sample) of the platelets, then $D = D_{hkl} \cos\alpha_{hkl}$, where α_{hkl} is the acute angle formed by the normal to the (*hkl*) planes and the normal to the platelets. Assuming that the broadening is mainly of Lorentzian character, then the

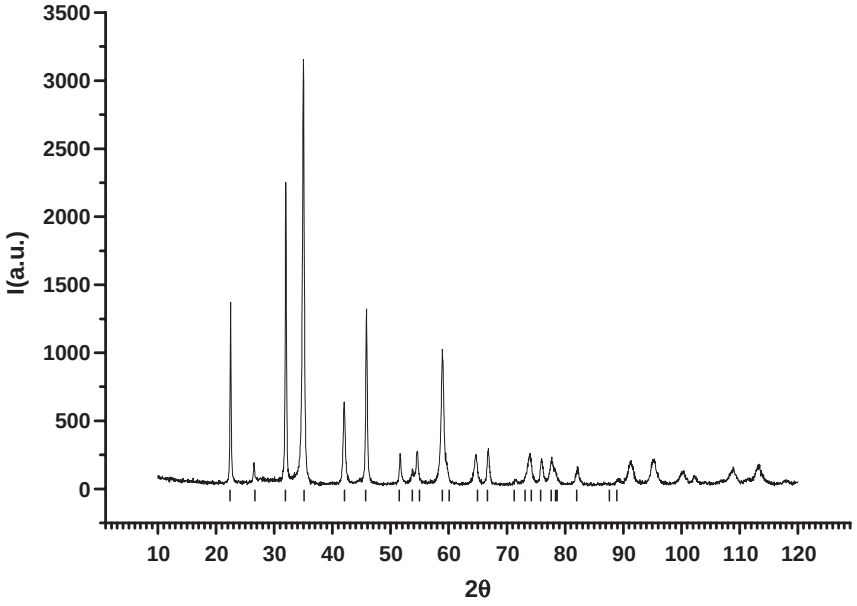

Fig. 4. High resolution X-ray diffractograms of a batch of 3 g of $LaNiO_2$ obtained by addition of 6 smaller samples.

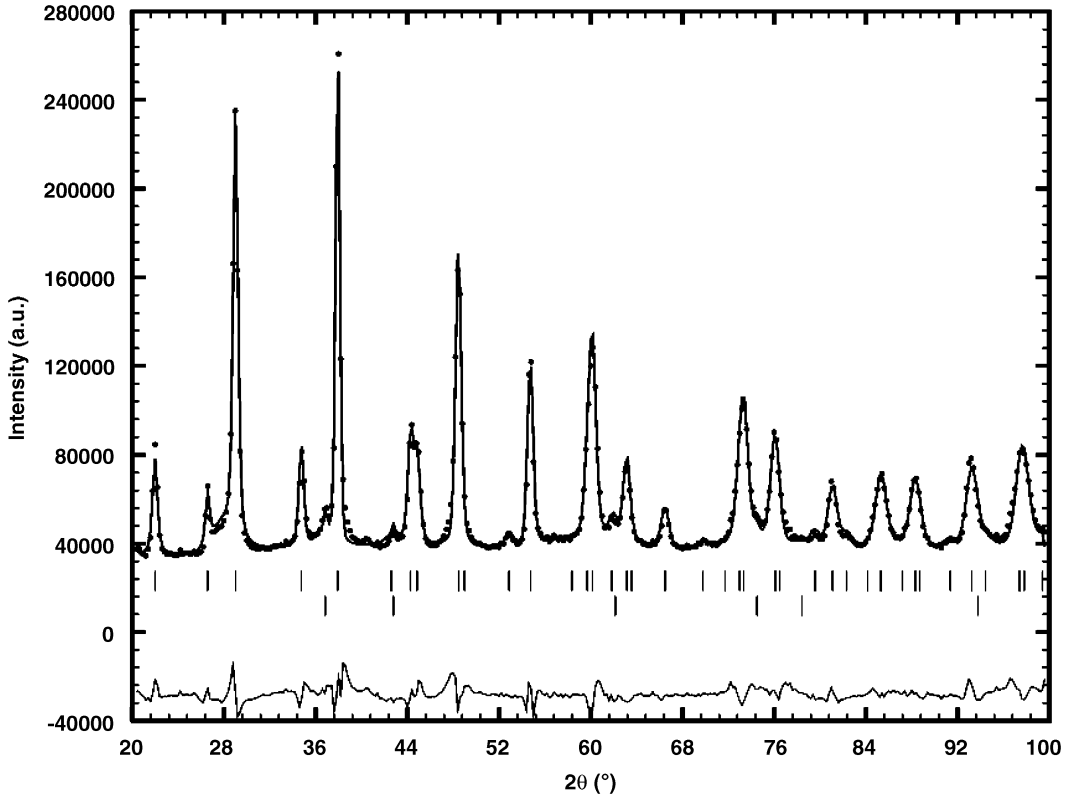

Fig. 5. Neutron powder diffraction pattern for $LaNiO_2$ at 300 K ($\lambda = 1.28$ Å). The drawn pattern refers to the experimental data. The difference between the experimental data and the calculated fit is plotted in the lower part of the figure. Vertical bars indicate calculated Bragg peak positions for (*hkl*) reflections. The second row of bars corresponds to the Bragg peak positions of the minority impurity Ni phase.

FWHM is given (in degrees) by

$$\mathrm{FWHM}_L = 360\lambda \cos \alpha_{hkl}/(\pi^2 D \cos \theta) = S_z \cos \alpha_{hkl}/\cos \theta, \quad (4)$$

where S_z is the parameter refined by FULLPROF from which the average thickness D can be obtained. This Lorentzian broadening when added to the instrumental Lorentzian component reproduces the experimental

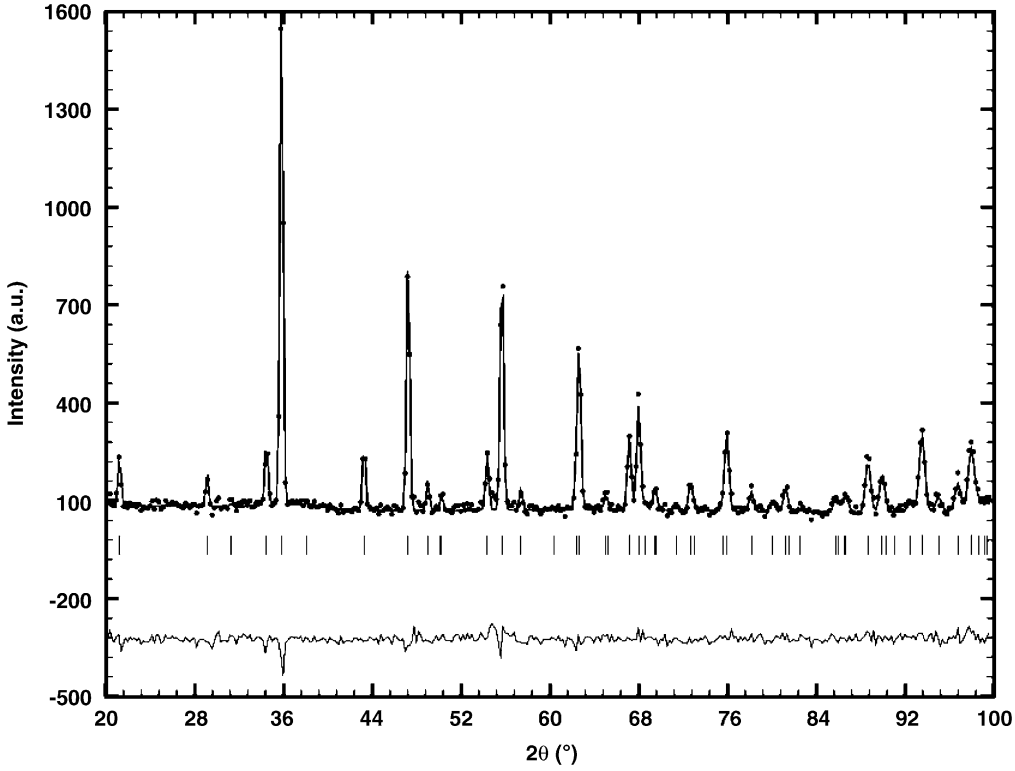

Fig. 6. Neutron powder diffraction pattern for Al_2O_3 at 300 K ($\lambda = 1.28$ Å). This reference diffraction pattern has been recorded in the same conditions as the one plotted on Fig. 4.

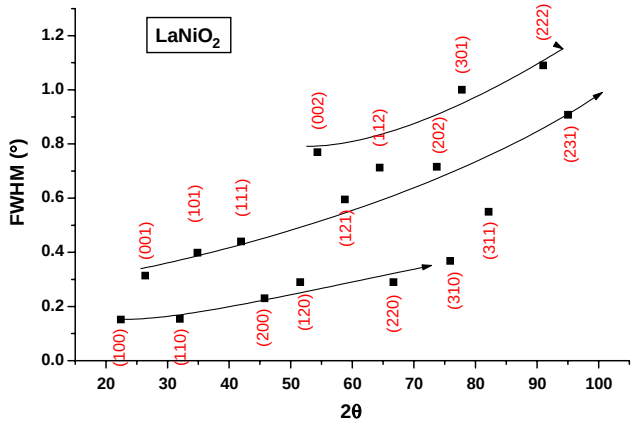

Fig. 7. Anisotropic X-ray line broadening in $LaNiO_2$.

Voigt peak shape (approximated by the Pseudo–Voigt function). The value obtained for the volume averaged thickness is $D = 200(17)$ Å. The precise nature of the defects given rise to the lack of long-range coherence of crystallites along the [001] direction is not known at present. An anisotropic broadening of the Bragg reflections has already been observed in several compounds prepared by low temperature de-oxygenation and particularly in nickelates and cobaltites [13,15,24–26]. This anisotropic line shape broadening most probably originates from the topotactic transformation involved in the oxygen de-intercalation process used to convert $LaNiO_3$ into $LaNiO_2$. In this respect, it must be emphasized that the X-ray pattern of the starting $LaNiO_3$ phase did not exhibited such peak broadening. One can perhaps speculate that due to the stronger La–O bonds than Ni–O bonds, one can expect that going from $LaNiO_3$ to $LaNiO_2$, the oxygen is removed from the Ni planes and then the structure brakes up along the [001] direction, then contributing to smaller coherent domains along [001] than along [100].

It is worth to note that attempts to refine the occupancy of all sites were performed but that no significant deviation from $LaNiO_2$ stoichiometry has been obtained. The occupancy for Ni was found to be 0.96(5) and that of oxygen 1.08(6) that is not significant deviations. In the same way, the possibility of a coexistence of a perfect infinite layer model NiO_2–La–NiO_2 with defective NiO_2–LaO–NiO_2 regions leading to an overall excess stoichiometry, as reported by Hayward et al. [16], has been herein checked. Unlike their results, a good fit of the diffraction pattern has been obtained without addition of a more complex description of the $LaNiO_2$ phase. Consequently, the final calculation is based on a full occupancy of the La, Ni and O sites. In the refinement procedure, Ni metal was introduced as a secondary phase; in any case, the calculated amount is 0.3 ± 0.02 weight percent. One could think that the removal of some Ni from the [...La/NiO_2/La...] sequence along the c axis must be accompanied by a

redistribution of the oxygen atoms toward the defective La planes and would induces the formation of corresponding pairs of LaO/LaO planes, typical of the intergrowth structure of La_2NiO_4. Even if the presence of an La_2NiO_4 extra-phase was not detected, the formation of some local La_2NiO_4-like defects is not precluded in agreement with the disproportionation of $LaNiO_2$ to Ni and La_2NiO_4 reported by Hayward et al. [16]. The experimental and calculated diffractograms of the final calculation are shown in Fig. 5 and the corresponding parameters and agreement factors are reported in Table 1.

The main M–O, M–M and O–O distances calculated in the structure of $LaNiO_2$, are reported in Table 2. The four Ni–O bond lengths (1.98 Å) are the same as found previously in $LaNiO_2$ (16). Of interest is the significant anisotropy of the La–La and Ni–Ni distances. In both cases, the two apical one are much shorter (3.37 Å) than the four in plane one (3.96 Å). The apical La–La distances are significantly shorter than the mean corresponding value in La_2O_3: 3.94 Å (27). It can be reasonably assumed that there will be a decrease of the La^{3+}–La^{3+} repulsive forces in the $LaNiO_2$ justifying the La–La shortening. As previously emphasized in the intergrowth oxides (27), this will play an important role in the bidimensionality of the structure and further in the metastability of $LaNiO_2$.

Table 1
Structural parameters of $LaNiO_2$ from NPD refinement

Temperature	290 K
Instrument	*D1B*
Wavelength (Å)	1.28
La 1*d* (x, y, z)	(0.5,0.5,0.5)
Ni 1*a*(x, y, z)	(0,0,0)
O 2*f* (x, y, z)	(0,0.5,0)
B_{La} (Å^2)	0.4 (2)
B_{Ni} (Å^2)	0.5 (1)
B_O (Å^2)	1.1 (1)
a (Å)	3.959 (1)
c (Å)	3.375 (1)
R_{Bragg} (%)	6.7
R_{wp} (%)	5.11
R_p (%)	3.97
R_{exp} (%)	0.43

SG(123), *P*4/*mmm*.

Table 2
Main interatomic distances at room temperature in $LaNiO_2$

Distances (Å)	La	Ni	O
La	4 × 3.959(1) 2 × 3.375(1)	8 × 3.268(3)	8 × 2.600(3)
Ni	8 × 3.268(3)	4 × 3.959(1) 2 × 3.375(1)	4 × 1.980(1)
O	8 × 2.600(3)	4 × 1.980(1)	2 × 3.375(1) 4 × 2.800(1)

A careful examination of the neutron diffraction background (Fig. 8) reveals the existence of some modulation in the range $2\theta = 28°$. Such feature is also visible in the X-ray diagram in the corresponding range $2\theta = 33°$. The background intensity of neutron diffractograms includes a contribution of elastic diffuse scattering, coming from a local static structural order [28]. Note that in the neutron diffraction pattern here recorded at room temperature in a regular vanadium container, the pattern is free from any diffuse scattering from the container, thus allowing a careful examination of the contribution due to the sample. It is well known that such a phenomenon gives evidence for the occurrence of short range ordering suggesting a possible second phase. This is not so surprising in the structure of an oxide, which is synthesized by a low temperature procedure. Such modulation effects have been identified in the neutron diffraction background of highly oxygen-conductive oxides and in Al_2O_3 treated at high temperature [29–32] and in the X-ray scattering background as well, for example in perovskite-like intergrowth type aluminate [33].

The Debye formula [28] can be used to express the contribution of a static structural order to the diffuse elastic scattering. It exhibits a first pronounced maximum for $Q_{max} = (2\pi \times 1.23)/d_m$, where d_m is a preferred pair distance. In our case, the modulation has a maximum at $Q\sharp$ 2.41 Å^{-1}, then it corresponds to a preferred pair distance close to 3.22 Å. Looking for metals able to pair at this distance points to two groups: (La–Ni) 8 distances of 3.26 Å in $LaNiO_2$ (see Table 2) and (La–La) one distance between LaO layers (3.25 Å) in the c direction of La_2NiO_4 [27]. Clearly, the former case cannot be considered resulting in a local ordering, since the La–Ni pairs are eaqually spread over the whole structure of $LaNiO_2$. On the contrary, the later case, i.e., La–La pairing along c corresponds to a local ordering induced by the removal of Ni atoms, as mentioned hearabove to account for the presence of the extra Ni phase.

Preliminary magnetization measurements with an SQUID magnetometer show a behaviour related to the strong magnetic contribution from Ni impurity (0.3 wt%) and complex $M(T)$ under low field. Attempts to subtract the contribution of Ni to that of the sample was not done.

4. Conclusion

A single $LaNiO_2$ phase sample is synthesized by controlled reduction under H_2 at 310 °C. Its structure is refined from NPD data taking into account an

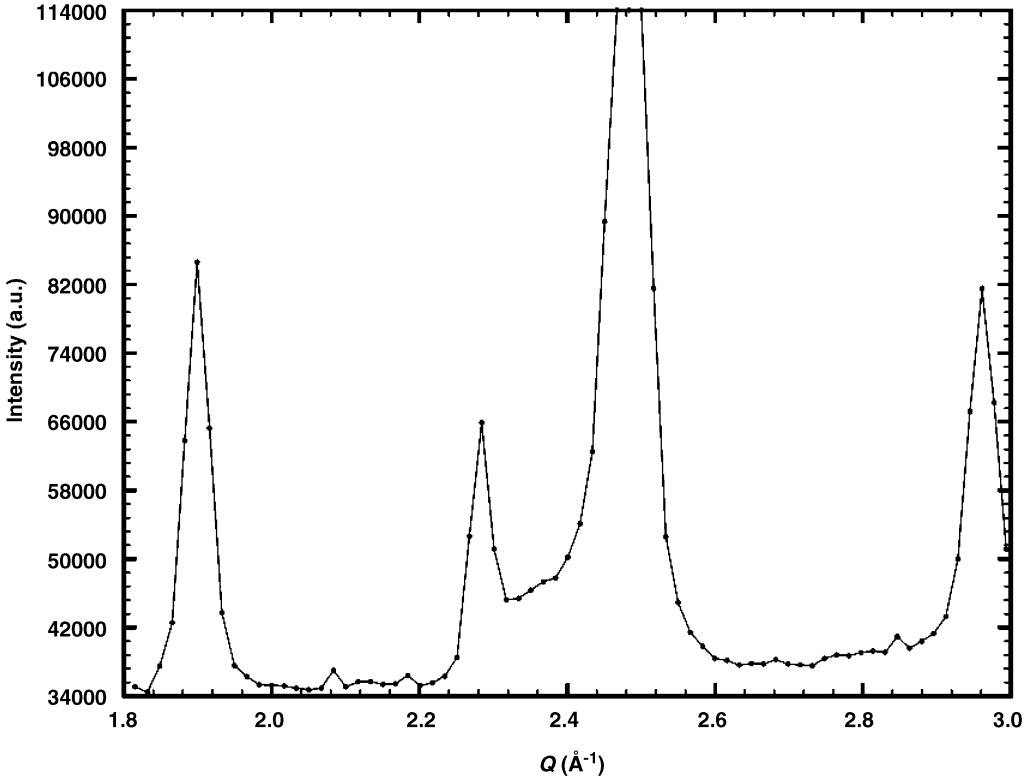

Fig. 8. Details of the neutron powder diffraction pattern $LaNiO_2$ at room temperature versus $Q = 4\pi \sin\theta/\lambda$ ($\lambda = 1.28$ Å) showing a large diffuse peak in the background around 2.41 $Å^{-1}$ (due to short range order with pair distances around 3.22 Å). Note that the container contribution is negligible (vanadium container).

anisotropic line broadening that is clearly evidenced. It is ascribed to the existence of coherent domains with different size according to the direction, i.e., 20 nm along [001], larger than 100 nm in the perpendicular direction. These domains are apparently linked with the reduction process giving rise to $LaNiO_2$. A modulation of the neutron diffraction background is observed, in connection with a cationic local ordering. It is suggested to correspond to small La_2NiO_4 particles expected to form because of an exsolution of Ni during the reduction process. Unfortunately, it probably results in a metastable phase that degrades at room temperature after several months.

Acknowledgments

The Institut Laue Langevin is warmly acknowledged for providing the neutron facilities as well as the CNRS for the use of the CRG–D1B instrument. Dr. A. Sulpice is thanked for preliminary measurements of magnetisation and fruitful discussions.

References

[1] Q. Feng, M. Hirasawa, K. Yanagisawa, Chem. Mater. 13 (2) (2001) 290.
[2] G. Gonzales, A. Sarzazu, R. Villalba, Mater. Res. Bull. 35 (14–15) (2000) 2295.
[3] A. Ibarra-Pales, M. Anne, P. Strobel, J. Solid State Chem. 160 (1) (2001) 108.
[4] S.V. Trukhanov, I.O. Troyanchuk, M. Hervieu, H. Szymczak, K. Barner, Phys. Rev. B 66 (18) (2002) 184421–184424.
[5] A. Stein, S.W. Keller, T.E. Mallok, Science 259 (1993) 1558.
[6] J.N. Lalena, R.A. McIntyre, B.L. Cushing, K.A. Thomas, J.L. Heintz, C.T. Seip, C.J. O'Connor, J.B. Wiley, Solid State Chem. Inorg. Mater. II-Symp. 99 (1999) 404.
[7] M. Crespin, P. Levitz, L. Gatineau, J. Chem. Soc. Fraday Trans. 79 (1983) 1181.
[8] M. Crespin, J.M. Bassat, P. Odier, P. Mouron, J. Choisnet, J. Solid State Chem. 84 (1990) 165.
[9] M. Crespin, C. Landron, J.P. Odier, M. Bassat, P. Mouron, J. Choisnet, J. Solid State Chem. 100 (1992) 281.
[10] M.J. Martinez-Lope, M.T. Casais, J.A. Alonso, J. Alloys Compds. 275–277 (1998) 109.
[11] A. Manthiran, J.P. Tang, V. Manivannan, J. Solid State Chem. 148 (1999) 499.
[12] P. Lacorre, J. Solid State Chem. 97 (1992) 495.
[13] R. Retoux, J. Rodriguez-Carvajal, P. Lacorre, J. Solid State Chem. 140 (1998) 307.
[14] F. Dubois, P. Odier, J. Choisnet, J. Mater. Chem. 13 (2003) 1.
[15] T. Siegrist, S.M. Zahurak, D.W. Murphy, R.S. Roth, Nature 334 (1988) 231.
[16] M.A. Hayward, M.A. Green, M.J. Rossdeinsky, J. Sloan, J. Am. Chem. Soc. 121 (1999) 8843.
[17] P. Odier, M. Munickan, M. Crespin, F. Dubois, P. Mouron, J. Choisnet, J. Mater. Chem. 12 (5) (2002) 1370.
[18] http://www.ill.fr, Yellow Book.
[19] J. Rodriguez Carjaval, Physica B 192 (1993) 55.

[20] L.B. McCusker, R.B. Von Dreele, D.E. Cox, D. Louer, P. Scardi, J. Appl. Crystallogr. 32 (1999) 36.
[21] V.F. Sears, Neutron News 3 (3) (1992) 26.
[22] F. Gotor-Martinez, P. Odier, O. Isnard, unpublished data.
[23] E.F. Bertaut, Acta Crystallogr. 5 (1952) 117.
[24] J.A. Alonso, M.J. Martinez-Lope, J.L. Garcia-Munoz, M.T. Fernandez-Diaz, J. Phys.: Condens. Mater. 9 (1997) 6417.
[25] M.A. Hayward, M.J. Rosseinsky, Chem. Mater. 12 (2000) 2182.
[26] J. Rodriguez-Carvajal, M.T. Fernandez-Diaz, J.L. Martinez, J. Phys. Condens. Matter 3 (1991) 3215.
[27] J. Choisnet, J. Solid State Chem. 147 (1999) 379.
[28] A. Guinier, Théorie et Techniques de la Radiocristallographie, Editions Dunod, Paris, 1964.
[29] R.N. Vannier, F. Abraham, G. Nowogrocki, G. Mairesse, J. Solid State Chem. 142 (1999) 294–304.
[30] F. Goutenoire, O. Isnard, R. Retoux, P. Lacorre, Chem. Mater. 12 (2000) 2575.
[31] F. Goutenoire, O. Isnard, E. Suard, O. Bohnke, Y. Laligant, R. Retoux, P. Lacorre, J. Mater. Chem. 11 (2001) 119.
[32] P. Aldebert, A.J. Dianoux, J.P. Traverse, J. Phys. 40 (1979) 1005.
[33] I. Zvereva, Yr. Smirnov, J. Choisnet, Mater. Chem. Phys. 60 (1999) 63.